

# Modeling and analysis of transients in periodic gratings. II. Resonant wave scattering

Kostyantyn Y. Sirenko,\* Yuriy K. Sirenko, and Nataliya P. Yashina

*Institute of Radiophysics and Electronics of National Academy of Sciences of Ukraine, 12 Acad. Proskura str., Kharkiv 61085, Ukraine*

\*Corresponding author: kostik13@gmail.com

Received November 9, 2009; accepted January 3, 2010;  
posted January 13, 2010 (Doc. ID 119695); published February 25, 2010

In this paper we represent a number of new physical results obtained using time domain methods and based on equivalent replacement of initially open electrodynamic problems with closed ones. These results prove the high efficiency and reliability of the approach, being grounded in our companion paper in this issue. © 2010 Optical Society of America

OCIS codes: 000.3860, 050.1950, 050.1755, 050.5745.

## 1. INTRODUCTION

In [1] we have built a system of exact absorbing boundary conditions for correct and effective truncation of the computational domain of 2-D initial boundary-value problems in the theory of gratings. This result allows us to implement equivalent replacement of initially open problems [formulas (3) in [1]] with closed ones. Standard discretization of these closed problems with the finite-difference method [2] using a uniform rectangular mesh attached to Cartesian coordinates  $g = \{y, z\}$  leads to explicit computational schemes with uniquely defined mesh functions  $U(j, k, m) \approx U(y_j, z_k, t_m)$  (from here on we use the same notation as in [1]). The approximation error is  $O(\bar{h}^2)$ ,  $\bar{h}$  is the mesh width in spatial coordinates,  $\bar{l} = \bar{h}/2$  for  $\vartheta = \max_{g \in \mathbf{Q}_L} [\varepsilon(g)\mu(g)] < 2$  or  $\bar{l} < \bar{h}/2$  for  $\vartheta \geq 2$  is the mesh width in time variable  $t$ ,  $y_j = j\bar{h}$ ,  $z_k = k\bar{h}$ , and  $t_m = m\bar{l}$ . The range of  $j$ ,  $k$ , and  $m$  integers depends on the size of  $\mathbf{Q}_L$  areas and the length of interval  $[0; T]$  of the observation time  $t$ :  $g_{jk} \in \mathbf{Q}_L$  and  $t_m \in [0; T]$ ;  $g_{jk} = \{y_j, z_k\}$ . The condition providing uniform boundedness of the approximate solutions  $U(j, k, m)$  with decreasing  $\bar{h}$  and  $\bar{l}$  is met [formula (1.50) in [3]]. Hence, in view of [4], the finite-difference computational schemes are stable, and the mesh functions  $U(j, k, m)$  tend to solutions  $U(g_{jk}, t_m)$  of original problems. The relevant test problems' solutions and other independent results serve to confirm the statement (for example, Section 4.6.1 in [3]).

Nonlocal and local absorbing conditions derived for the grating problems were tested to determine that errors introduced by their implementation into explicit finite-difference schemes of the second approximation order do not exceed the standard sampling error. They are much smaller than the errors caused by the use of classical approximate absorbing boundary conditions [5,6] of the first, second, and third approximation orders. Also, in contrast, they exhibit almost no growth with time  $t$ . We make a

special emphasis of this point because long-duration time intervals are required for trustworthy analysis in the resonant case.

## 2. ELECTRODYNAMIC CHARACTERISTICS OF GRATINGS

Analysis of infinite single-period gratings rests on the numerical solution of problems of type (36) from [1]. The transfer to finite domain of analysis  $\mathbf{Q}_L$  is assisted by exact absorbing conditions (41), (42) from [1] (see also Fig. 2 in [1]).

Let us represent the total field  $U(g, t)$  in the form  $U(g, t) = U^i(g, t) + U^s(g, t)$ ;  $g \in \mathbf{A}$  and  $U(g, t) = U^s(g, t)$ ;  $g \in \mathbf{B}$  where  $U^i(g, t)$  is the field produced in the channel  $\mathbf{R}$  by some sources  $\tilde{F}(g, t)$ ,  $\tilde{\phi}(g)$ , and  $\tilde{\psi}(g)$ . Then [see formulas (4) and (44) in [1]],

$$U^s(g, t) = \sum_{n=-\infty}^{\infty} u_n(z, t) \mu_n(y) \text{ and} \\ U^i(g, t) = \sum_{n=-\infty}^{\infty} v_n(z, t) \mu_n(y); \quad t \geq 0. \quad (1)$$

$U(g, t) = E_x(g, t)$  or  $U(g, t) = H_x(g, t)$  depending whether the field is  $E$ - or  $H$ -polarized. In domain  ${}_L\mathbf{Q} = \mathbf{A} \cup \mathbf{B}$  [see formulas (1.5) and (1.7) in [3]],

$$\partial \left\{ \begin{matrix} H_y \\ E_y \end{matrix} \right\} / \partial t = \mp \eta_0^{\mp 1} \frac{\partial U}{\partial z}, \quad \partial \left\{ \begin{matrix} H_z \\ E_z \end{matrix} \right\} / \partial t \\ = \pm \eta_0^{\mp 1} \frac{\partial U}{\partial y}; \quad \left\{ \begin{matrix} E\text{-case} \\ H\text{-case} \end{matrix} \right\}. \quad (2)$$

Then [cf. the representation (1)],

$$\begin{cases} H_{y(z)}^s \\ E_{y(z)}^s \end{cases} = \sum_{n=-\infty}^{\infty} u_n^{y(z)}(z,t) \mu_n^{y(z)}(y),$$

$$\begin{cases} H_{y(z)}^i \\ E_{y(z)}^i \end{cases} = \sum_{n=-\infty}^{\infty} v_n^{y(z)}(z,t) \mu_n^{y(z)}(\rho); \quad \begin{cases} E\text{-case} \\ H\text{-case} \end{cases}. \quad (3)$$

The spatial-temporal amplitudes  $u_n(z,t)$ ,  $v_n(z,t)$ , etc., in the representations (1) and (3) are also called the evolutionary basis elements of the corresponding signals [7,8]. They fully describe the dynamics of the  $U^s(g,t)$  ( $U(g,t)$ ) and  $U^i(g,t)$  pulsed waves propagating along the Floquet channel as well as their mode and spectral contents.

In  $\mathbf{Q}_L$  domain, the simulated process dynamics is estimated on the time dependences  $U(g,t)$ , referring to particular points  $g \in \mathbf{Q}_L$  as well as the point set  $\mathbf{Q}_L$  as a whole. In the latter case, current values of the complex

quantities  $U(g,t)$  are specified by the color of pixels (spatial mesh cells) throughout the computational domain  $\mathbf{Q}_L$ .

Let us attach domains  $\mathbf{A}$  and  $\mathbf{B}$  to the local coordinate system  $g_j = \{y_j, z_j \geq 0\}$ ;  $j=1,2$ , and boundary  $\mathbf{L}_j$  lies in plane  $z_j=0$  (see Fig. 2 in [1]). Then, starting from the values on the boundary  $\mathbf{L}_j$ , the diagonal transport operator  $Z_{0 \rightarrow z_j}(t)$  (see Section 3 in [1]) will calculate the spatial-temporal amplitudes  $u(z_j,t) = \{u_n(z_j,t)\}$  for any  $z_j \geq 0$  section of the corresponding regular channel  $\mathbf{R}$ . This means that [see also (1)–(3)] any electrodynamic characteristic of the grating is defined by amplitude sets  $\{u_n(z_j,t)\}_{z_j=0}$ ;  $j=1,2$  of the secondary pulsed field  $U^s(g_j,t)$  on the virtual boundaries  $\mathbf{L}_j$ .

Now let the grating be excited by a pulsed wave  $U_p^i(g_1,t) = v_p(z_1,t) \mu_p(y_1)$  coming from area  $\mathbf{A}$ ;  $\mathbf{Q}_L$  domain has no current sources. In this case relationship

$$\underbrace{P_1^s + P_2^s + P_1^{i \times s}}_1 + \underbrace{\frac{1}{2} \frac{\partial}{\partial t} \int_{\mathbf{Q}_L} \left( \eta_0 \mu |\vec{H}|^2 + \frac{\varepsilon}{\eta_0} |\vec{E}|^2 \right) dg}_2 + \underbrace{\frac{1}{\eta_0} \int_{\mathbf{Q}_L} \sigma |\vec{E}|^2 dg}_3 = -P_1^i \quad (4)$$

with ( $dg = dydz$ ) governs the balance of instant powers of the electromagnetic field. Namely, the instant power arriving at  $\mathbf{Q}_L$  across the boundary  $\mathbf{L}_1$  is the sum of total instant power (1) radiated across  $\mathbf{L}_j$  boundaries into  $\mathbf{L}_j \mathbf{Q}$  domain, instant power (2) accumulative in the  $\mathbf{Q}_L$  domain, and instant accepted power (3). Here,

$$P_j^{s(i)}(t) = \int_{\mathbf{L}_j} ([\vec{E}^{s(i)} \times \vec{H}^{s(i)}] \cdot \vec{n}_j) dy_j,$$

$$P_1^{i \times s}(t) = \int_{\mathbf{L}_1} [([\vec{E}^s \times \vec{H}^i] + [\vec{E}^i \times \vec{H}^s]) \cdot \vec{n}_1] dy_1,$$

$\vec{n}_j$  is the outward normal to  $\mathbf{Q}_L$  domain at the boundary  $\mathbf{L}_j$ , and  $\vec{E}^{s(i)}$  and  $\vec{H}^{s(i)}$  are the electric and magnetic fields of the waves  $U^s(g,t)$  ( $U^i(g,t)$ ) in domains  $\mathbf{A}$  and  $\mathbf{B}$ .

The amplitude-frequency characteristics  $\tilde{f}(k)$  (where  $k = 2\pi/\lambda$ ;  $\text{Re } k > 0$ ,  $\text{Im } k = 0$  is the wavenumber or some frequency parameter or simple frequency, and  $\lambda$  is the free space wavelength) come from the time characteristics  $f(t)$  by virtue of integral transformation

$$\tilde{f}(k) = \int_0^T f(t) e^{ikt} dt \leftrightarrow f(t), \quad (5)$$

where  $T$  is the upper limit of the interval  $[0; T]$  of the observation time  $t$ , and for all  $t > T$ , the function  $f(t)$  is assumed to be zero.

The frequency domain traditional characteristics  $R_{np}^{\mathbf{A}\mathbf{A}}(k)$  and  $T_{np}^{\mathbf{B}\mathbf{A}}(k)$  (see, for example, [9–11]) represent the conversion coefficients. The former indicates how the  $p$ th mode incident from part  $\mathbf{A}$  of Floquet channel  $\mathbf{R}$  converts into the  $n$ th reflection mode (synonymous with reflection coefficient). The latter shows how the  $p$ th mode arriving from domain  $\mathbf{A}$  transforms into the  $n$ th mode in domain  $\mathbf{B}$  (transition coefficient). Specifically

$$R_{np}^{\mathbf{A}\mathbf{A}}(k) = \left. \frac{\tilde{u}_n(z_1, k)}{\tilde{v}_p(z_1, k)} \right|_{z_1=0}, \quad T_{np}^{\mathbf{B}\mathbf{A}}(k) = \frac{\tilde{u}_n(z_2, k)|_{z_2=0}}{\tilde{v}_p(z_1, k)|_{z_1=0}}. \quad (6)$$

When the grating is excited by a propagating ( $\text{Im } \Gamma_p = 0$ ) or damped ( $\text{Im } \Gamma_p > 0$ ) monochromatic wave  $\tilde{U}_p^i(g, k) = \exp[i(\Phi_p y - \Gamma_p(z - L_1))]$  the total field in domain  $\mathbf{Q}_L = \mathbf{A} \cup \mathbf{B}$  is ([3])

$$\tilde{U}(g, k) = \begin{cases} \tilde{U}_p^i(g, k) + \sum_{n=-\infty}^{n=\infty} R_{np}^{\mathbf{A}\mathbf{A}} \exp[i(\Phi_n y + \Gamma_n(z - L_1))]; & g \in \mathbf{A} \\ \sum_{n=-\infty}^{n=\infty} T_{np}^{\mathbf{B}\mathbf{A}} \exp[i(\Phi_n y - \Gamma_n(z + L_2))]; & g \in \mathbf{B} \end{cases}, \quad (7)$$



$$v_0(L_1, t) = 4 \frac{\sin[\Delta k(t - \tilde{T})]}{(t - \tilde{T})} \cos[\tilde{k}(t - \tilde{T})] \chi(\tilde{T} - t) = F_1(t);$$

$$\Delta k = 0.7, \quad \tilde{T} = 50, \quad \bar{T} = 100.$$

Parameters  $\tilde{k}$ ,  $\Delta k$ ,  $\tilde{T}$ , and  $\bar{T}$  establish the central frequency of the signal  $U_0^i(g, t)$ , its spectral bandwidth ( $\tilde{k} \pm \Delta k$ ), delay time [the moment when the principal part of the pulse  $U_0^i(g, t)$  crosses boundary  $\mathbf{L}_1$ ], and duration. The short notation for signal  $U_0^i(g, t)$  is

$$U_0^i(g, t): \Phi = 0; \quad v_0(L_1, t) = F_1(t); \quad \tilde{k}, \quad \Delta k = 0.7,$$

$$\tilde{T} = 50, \quad \bar{T} = 100. \quad (11)$$

Having solved the corresponding initial boundary-value problems for any time  $0 < t \leq T$ ;  $T = 500$ , we can obtain the electro-dynamical characteristics of the structure [see Fig. 1(b)] in the frequency bands  $1.4 \leq k \leq 2.8$  [the central frequency of signal (11) is  $\tilde{k} = 2.1$ ] and  $2.8 \leq k \leq 4.2$  ( $\tilde{k} = 3.5$ ). Why do we halve the analyzed frequency interval  $1.4 \leq k \leq 4.2$ ? Because free oscillation field  $U(g, t)$ ,  $g \in \mathbf{Q}_L$ ,  $t > \bar{T}$  gets rid of the contribution from the threshold effect taking place at one of the threshold points  $k_n^\pm = \pm |\Phi_n|$  of the grating:  $k_{\pm 1}^+ \approx 1.56$  (for  $\tilde{k} = 3.5$ ) or  $k_{\pm 2}^+ \approx 3.13$  (for  $\tilde{k} = 2.1$ ).

In frequency band  $1.7 \leq k \leq 2.0$  and beyond point  $k_{\pm 1}^+ \approx 1.56$  (where the first high-order spatial propagating harmonics appear), the echelette grating manages to concentrate over 98% of the input energy delivered by a normally falling  $H$ -polarized plane wave  $\tilde{U}_0^i(g, k)$  in one of these harmonics (the minus first one) (see Fig. 1(b)). For these  $k$  values, the departure angle  $\alpha_{-1} = -\arcsin(\Phi_{-1}/k)$  of  $R_{-10}^{AA}(k)$ -amplitude harmonic from the grating is  $\alpha_{-1} = 66.8^\circ$  to  $\alpha_{-1} = 51.4^\circ$ . Beyond the second threshold point  $k_{\pm 2}^+ \approx 3.13$  a substantial part of the incident energy is given to the minus second spatial harmonic. But its  $W_{-20}^R(k)$  function does not grow as fast as  $W_{-10}^R(k)$  does, and it cannot achieve values as high.

At the frequency  $k = 2.89$  all the energy is uniformly distributed between the principal and the minus first spatial harmonics [ $W_{-10}^R(k) = W_{00}^R(k) = 0.5$  and  $W_{10}^R(k) = 0$ ;  $\alpha_0 = 0$  and  $\alpha_{-1} = 32.7^\circ$ ]. Compare with  $W_{10}^R(k) = W_{00}^R(k) \approx 0.49$ ,  $W_{-10}^R(k) \approx 0.02$ , and  $\alpha_1 = -31.2^\circ$  at the frequency  $k = 3.015$ . From an asymmetric echelette grating, we can also get symmetric channels to radiate the input energy. Thus  $W_{10}^R \approx W_{-10}^R \approx 0.46$ ,  $W_{00}^R(k) \approx 0.08$ , and  $\alpha_{\pm 1} = \pm 30.3^\circ$  at the point  $k = 3.098$ .

Let us consider a reflective grating under normal incidence of  $E$ - or  $H$ -polarized quasi-monochromatic wave  $U_0^i(g, t)$ . The energy fluxes directed to the side channels can be visualized via the calculation of the spatial-time distribution of  $H_z(g, t)$  or  $E_z(g, t)$  values corresponding to the field  $U(g, t)$ ;  $g \in \mathbf{Q}_L$ . Indeed, the excitation with a quasi-monochromatic wave whose spectral amplitudes decrease rapidly as frequency  $k$  moves off  $k = \tilde{k}$  makes it possible to minimize the angular widening of the side channels. Then the  $z$  components of the incident wave field  $U_0^i(g, t)$  and of the total field's  $U(g, t)$  part traveling toward it are equal to zero. Figure 2 plots the solutions of

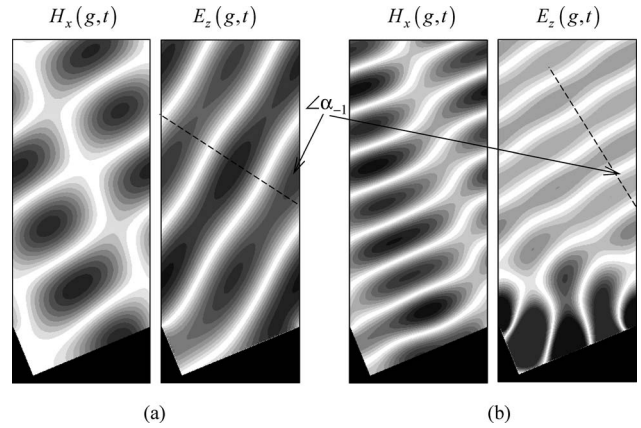


Fig. 2. Echelette excitation by quasi-monochromatic pulsed wave (12) with central frequency (a)  $\tilde{k} = 1.85$  and (b)  $\tilde{k} = 2.89$ . Parameters  $H_x(g, t)$  and  $E_z(g, t)$  spatial distributions,  $g \in \mathbf{Q}_L$  at time  $t = 101$ .

the initial boundary-value problems of the echelette grating excited by the quasi-monochromatic wave

$$U_0^i(g, t): \Phi = 0; \quad v_0(L_1, t) = \cos[\tilde{k}(t - \tilde{T})] \chi(\tilde{T} - t) = F_2(t);$$

$$\tilde{k}, \quad \tilde{T} = 0.5, \quad \bar{T} = 300 \quad (12)$$

with the central frequencies  $\tilde{k} = 1.85$  [Fig. 2(a)] and  $\tilde{k} = 2.89$  (Fig. 2(b)). Let us recollect (see above) that  $W_{-10}^R(k) > 0.98$  and  $\alpha_{-1} = 57.7^\circ$  at the frequency  $k = 1.85$ , and  $W_{-10}^R(k) = 0.5$  and  $\alpha_{-1} = 32.7^\circ$  at  $k = 2.89$ . These  $\alpha_{-1}$  values are shown in those parts of Fig. 2 where the spatial distribution of  $E_z(g, t)$  is plotted:  $g \in \mathbf{Q}_L$ ,  $t = 101$ . They give a sufficiently accurate picture of the orientation of side channels drawing energy away from the grating.

Reflective gratings excited by an oblique incident ( $\sin \alpha_0^i = \Phi_0/k \neq 0$ )  $E$ - or  $H$ -polarized plane wave  $\tilde{U}_0^i(g, k)$  can concentrate most of the energy input into one of the high-order spatial harmonics  $R_{n0}^{AA}(k) \exp[i(\Phi_n y + \Gamma_n(z - L_1))]$ , with  $n \neq 0$  of the secondary field  $\tilde{U}^s(g, k) = \tilde{U}(g, k) - \tilde{U}_0^i(g, k)$ ,  $g = \{y, z\} \in \mathbf{A}$  [see formula (7) and [9–11]]. The propagation direction of this harmonic according to the angle  $\alpha_n = -\arcsin(\Phi_n/k)$  is different from the direction of the specular reflection wave  $R_{00}^{AA}(k) \exp[i(\Phi_0 y + \Gamma_0(z - L_1))]$ ,  $\alpha_0 = -\alpha_0^i$ . If  $W_{n0}^R(k) = 1$ , we say that a *total nonspecular reflection effect* takes place. Let  $n = -m$  and

$$W_{-m0}^R(k) = 1, \quad kl \sin(\alpha_0^i) = \pi m. \quad (13)$$

If condition (13) holds [see also formula (10)] for some values of  $k$ , it is said that the *effect of total autocollimation reflection* takes place on the minus  $m$ th spatial harmonic, implying that all the energy is concentrated into the plane wave traveling toward the incident wave  $\tilde{U}_0^i(g, k)$ . In the autocollimation regime  $\Phi = m/2$ , the propagation constants  $\Gamma_n$  of specular ( $n = 0$ ) and autocollimation ( $n = -m$ ) harmonics coincide at the same time as  $\Phi_0 = -\Phi_{-m}$ .

The effect of total or nearly total autocollimation reflection on the minus first spatial harmonic can be both spread over a wide band and be retained within a narrow band. For example, Fig. 3(b) shows that for geometry 1 the  $0.85 \leq k \leq 1.85$  bandwidth where  $W_{-10}^R(k) \geq 0.95$

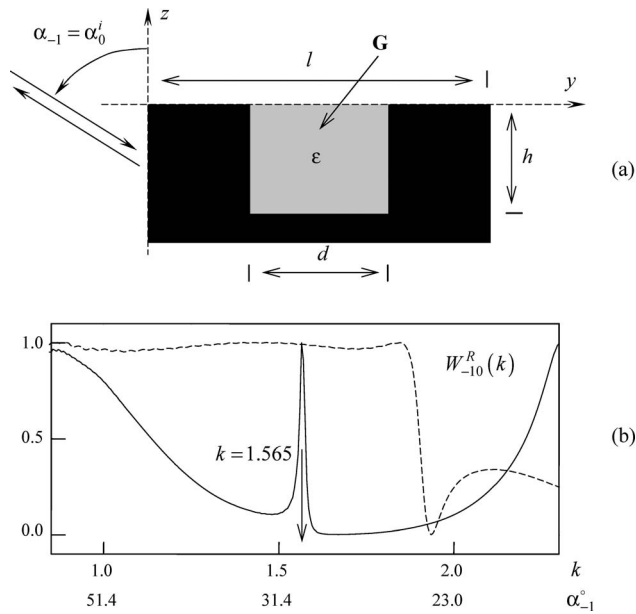


Fig. 3. *H*-polarization; autocollimation reflection on the minus first spatial harmonic: (a) Grating geometry :  $L_1=8.4$ ;  $1-l=4.02$ ,  $h=1.0$ ,  $d=2.02$ ,  $\epsilon=1$ ;  $2-l=4.02$ ,  $h=1.28$ ,  $d=1.62$ ,  $\epsilon=2$ ); (b) reflection efficiency: geometry 1, dashed curve; geometry 2, solid curve.

amounts up to 74%. In the first case, the effect is realized because of low-Q oscillations of the first family in domain  $\mathbf{G}$  [3,12], namely, the oscillations on  $TEM$ - or  $H_{01}$ -waves in  $d$ -wide parallel-plate waveguide segments. In the second case, the responsibility for maintenance of the effect rests on larger-Q oscillations of  $E_{0n}$ - ( $n \geq 1$ ) or  $H_{0n}$ -waves ( $n \geq 2$ ). But in any case the limit value can be reached only when no more than two—the zeroth and the minus first—spatial harmonics propagate without attenuation in the reflection zone of the periodic structure.

The data reported in Fig. 3 were obtained by studying the grating response to excitation by the pulsed *H*-polarized wave

$$U_0^i(g,t): \Phi = 0.5, \quad v_0(L_1,t) = F_1(t), \quad \tilde{k} = 1.55, \\ \Delta k = 0.75, \quad \tilde{T} = 50, \quad \bar{T} = 100. \quad (14)$$

The band  $0.8 \leq k \leq 2.3$ , where spectral amplitudes of the signal (14) reach their maxima, does not include the

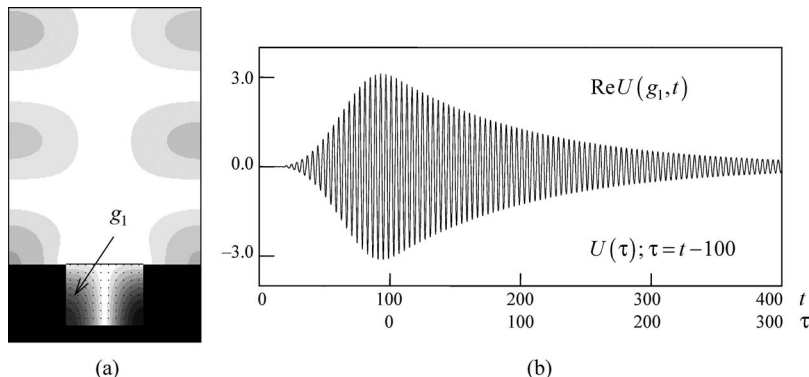


Fig. 4. Reflective grating excitation (geometry 2) by an *H*-polarized quasi-monochromatic wave  $U_0^i(g,t)$ :  $\Phi=0.5$ ;  $v_0(L_1,t)=F_2(t)$ ;  $\tilde{k}=1.565$ ,  $\tilde{T}=0.5$ ,  $\bar{T}=100$ : (a) The  $H_x(g,t)$  spatial distribution,  $g \in \mathbf{Q}_L$  at the time  $t=205$ ; (b) functions  $\text{Re}U(g_1,t)$  and  $U(\tau)$ .

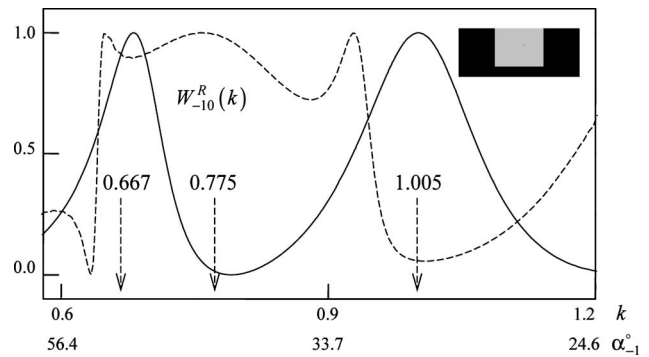


Fig. 5. Autocollimation reflection efficiency on the minus first spatial harmonic: *H*-polarization, dashed curve; *E*-polarization, solid curve;  $l=2\pi$ ,  $h=4.3$ ,  $d=3.8$ ,  $\epsilon=2$ .

threshold points  $k_0^+ = k_{-1}^+ \approx 0.782$  and  $k_1^+ = k_{-2}^+ \approx 2.35$ . Therefore in the free oscillation field  $U(g,t)$ ;  $t > 100$ , the oscillation on  $E_{01}$ -waves in the grating with geometry 2 is clear enough—we can see that from the  $H_x(g,t)$  spatial distribution,  $g \in \mathbf{Q}_L$  at any time  $t \geq 200$ . Evidently this oscillation is the only one characterized by high Q-factor whose complex eigenfrequency  $\tilde{k}$  is under the segment  $0.8 \leq k \leq 2.3$  of the real axis  $k > 0$ . It seems that this oscillation is responsible for the total autocollimation reflection at the frequency  $k=1.565$  [see Fig. 3(b)]. This hypothesis is based on an analysis of the grating’s response to the excitation by a quasi-monochromatic *H*-polarized wave  $U_0^i(g,t)$  with the central frequency  $\tilde{k}=1.565$  (see Fig. 4). The spectral amplitudes of function  $U(\tau) = \text{Re} U(g_1,t)$ ,  $\tau = t - 100 > 0$  are at their maxima in the small vicinity of the point  $k=1.569$ ; its envelope  $f(\tau)$  obeys the equation  $f(\tau) = \pm 3.12 \exp(-0.0088\tau)$ . This means (see [13]) that free oscillation on the  $E_{01}$ -waves [see Fig. 4(a)] fits the eigenfrequency  $\tilde{k} \approx 1.569 - i0.0088$ .

Reflective gratings can be used as dispersive elements to make effective polarization selection of signals. Let us refer to the situation reported in Fig. 5. At the frequency  $k=0.775$ , 99% of the input energy is drawn toward the incident plane wave when it is *H*-polarized and only 1% when the incident plane wave is *E*-polarized. At the frequency  $k=1.005$ , the main channels of energy withdrawal of *E*- and *H*-polarized waves are interchanged:  $W_{-10}^R(k) = 0.05$  for *H*-polarization and  $W_{-10}^R(k) = 1.0$  for *E*-polarization. At the frequency  $k=0.667$ ,  $W_{-10}^R(k) = 0.92$

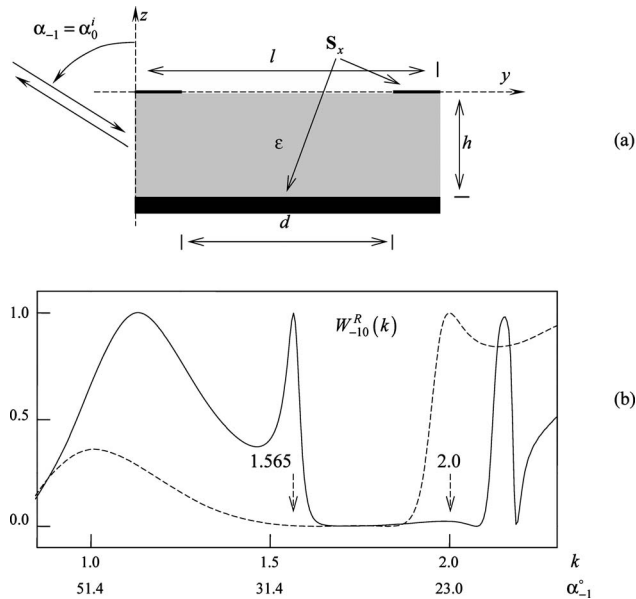


Fig. 6. Autocollimation reflection efficiency on the minus first spatial harmonic: (a) Grating geometry ( $l=4.02$ ,  $h=1.42$ ,  $d=2.78$ ,  $\epsilon=2$ , perfectly conducting strip thickness is  $0.04$ ,  $L_1=8.4$ ); (b) reflection efficiency:  $H$ -polarization, dashed curve;  $E$ -polarization, solid curve.

for both polarizations. The portion of energy contributed to the specular reflection spatial harmonics is by virtue of the equation  $W_{-10}^R(k) + W_{00}^R(k) = 1.0$ : in the band  $0.5 < k < 1.5$ , only the principal and the minus first harmonics of the secondary field  $\tilde{U}^s(g, k)$  travel without attenuation in domain **A**.

A grating formed by thin metal strips lying on a dielectric substrate backed by a perfectly conducting screen fully separates polarizations when the autocollimation reflection regime happens on the minus first spatial harmonic. Figure 6 shows that at  $k=1.565$  all the energy delivered by an  $E$ -polarized wave goes to the minus first spatial harmonic ( $W_{-10}^R(k)=1.0$ ). When the incident wave is  $H$ -polarized all the energy concentrates into the specular reflection harmonic ( $W_{-10}^R(k)=0.0$ ). At  $k=2.0$  the separation of polarizations is not so fine. Here  $W_{-10}^R(k)=1.0$  in the case of  $H$ -polarization of the field and  $W_{-10}^R(k)=0.02$  ( $W_{00}^R(k)=0.98$ ) in the  $E$ -case.

#### 4. GRATINGS IN A PULSED WAVE FIELD

It is evident that complete analytic description of pulse deformations in regular and irregular Floquet channels is impossible without proper computational work. The figures obtained must be adequately interpreted. A treatment of this kind originated in [3,14]. Here we discuss some recent results based on the method reported in [1].

Four  $E$ -polarized sinusoidal plane waves  $\tilde{U}_0^i(g, k) = \exp(-ikz)$ ,  $\tilde{U}_0(g, k) = \exp(ikz)$ ,  $\tilde{U}_1(g, k) = -\exp(iky)$ , and  $\tilde{U}_{-1}(g, k) = -\exp(-iky)$  traveling in free space result in the field  $\tilde{E}_x(g, k)$  whose null surfaces at  $k = k_{\pm 1}^+ = 2\pi/l$  can be brought into coincidence with the surface  $\mathbf{S} = \mathbf{S}_x \times [|x| \leq \infty]$  of a symmetric echelette grating (see Fig. 1(a),  $\psi = 45^\circ$ ). This means that the total field originating when

the echelette grating is excited by the wave  $\tilde{U}_0^i(g, k)$  coincides (everywhere above the contour  $\mathbf{S}_x$ ) with the field  $\tilde{U}(g, k) = \tilde{U}_0^i(g, k) + \sum_{n=0,1,-1} \tilde{U}_n(g, k)$ . In this case waves  $\tilde{U}_n(g, k)$ ,  $n=0, \pm 1$  play the parts of principal, plus first, and minus first spatial harmonics of the secondary field  $\tilde{U}^s(g, k) = \tilde{U}(g, k) - \tilde{U}_0^i(g, k)$ . Usually in this way a reason is given for an explicit analytic solution of a scattering problem in the frequency domain; the existence of the solution is attributed to the so-called geometrical resonances [11]. Later we will see what this geometrical resonance (a frequency domain effect) can tell us about the solution of the corresponding scattering problem in the time domain.

Let us assume that a symmetric echelette grating is excited by  $E$ -polarized quasi-monochromatic wave  $U_0^i(g, t)$ :  $\Phi=0$ ,  $v_0(L_1, t) = F_2(t)$ ,  $\tilde{k} = 1.563 \approx k_{\pm 1}^+$ ,  $\tilde{T} = 0.5$ ,  $\bar{T} = 200$  (see Figs. 7 and 8). We will compare the spatial-temporal amplitudes of the signal  $U_0^i(g, t)$  and the principal spatial harmonics  $U_n(g, t) = u_n(z, t)\mu_n(y)$ ,  $n=0, \pm 1$  due to this signal in the reflection zone of the grating. Function  $v_0(L_1, t)$ , whose related spectral amplitudes do not exceed 0.3 beyond the narrow frequency band  $1.54 < k < 1.586$ , has a simple envelope and vanishes for all  $t > \bar{T}$ . The effective spatial duration of the signals  $U_0(g, t)$  and  $U_0^i(g, t)$  is practically the same, but the amplitude of  $U_0(g, t)$  gradually increases by action of the perturbation source. The main part of the pulse  $u_0(L_1, t)$  is followed by a short and fast decaying tail. The tails of the pulses  $u_{\pm 1}(L_1, t)$  are more powerful, which is probably due to the plus and the minus first harmonics being the principal components of the free oscillation field complying with the eigenfrequency  $\tilde{k}$

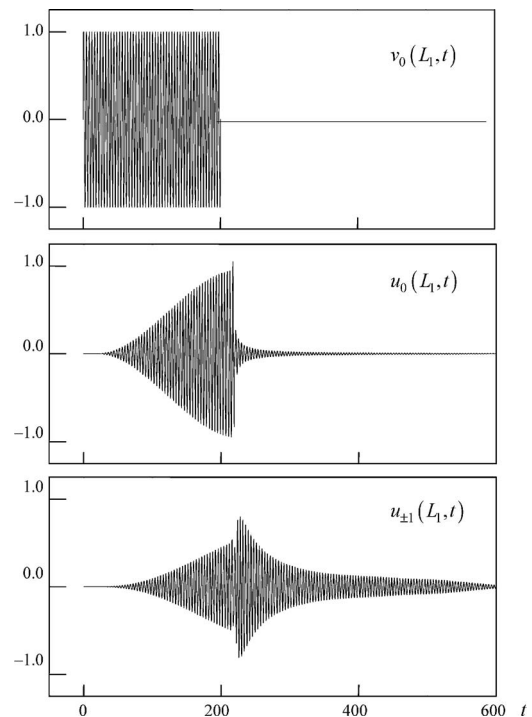


Fig. 7. Excitation of a symmetric echelette ( $\psi=45^\circ$ ,  $l=4.02$ ,  $L_1=7.8$ ) by a normally incident  $E$ -polarized quasi-monochromatic wave  $U_0^i(g, t)$ . The spatial-temporal amplitudes are shown for the  $U_0^i(g, t)$  wave and the principal spatial harmonics of the secondary field  $U^s(g, t)$  on the virtual boundary  $L_1$ .

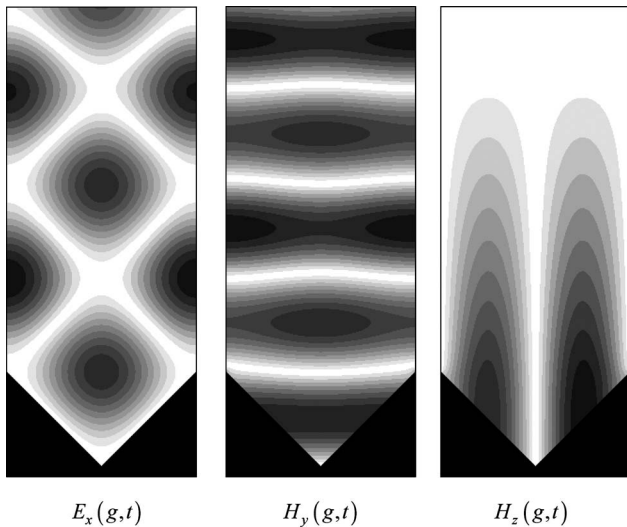


Fig. 8. (Complement to Fig. 7).  $E_x(g,t)$ ,  $H_y(g,t)$  and  $H_z(g,t)$  spatial distributions,  $g \in \mathbf{Q}_L$ ,  $t = 189.75$ .

( $\text{Re } \bar{k}$  is in close proximity to the threshold point  $k_{\pm 1}^+ \approx 1.563$ ).

The main carriers of the  $H_z(g,t)$  component of the field  $U(g,t)$  are  $U_{\pm 1}(g,t)$  waves. The  $H_y(g,t)$  main carriers are

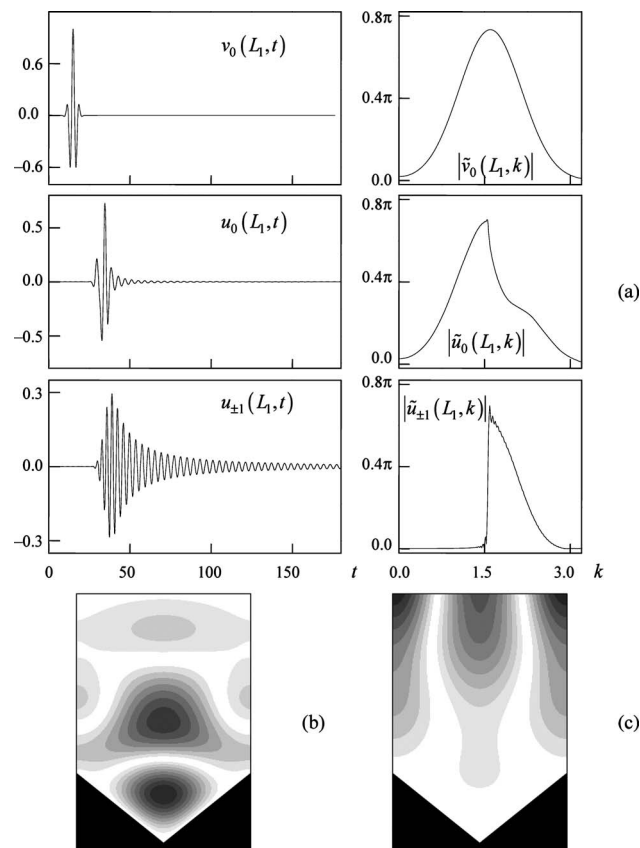


Fig. 9. Symmetric echelette excitation by a normally incident  $E$ -polarized Gaussian pulse  $U_0^i(g,t)$ : (a) The spatial-temporal and the spectral amplitudes are shown for the  $U_0^i(g,t)$  wave and the principal spatial harmonics of the secondary field  $U^s(g,t)$  on the virtual boundary  $L_1$ ; (b),(c) the  $E_x(g,t)$  spatial distribution,  $g \in \mathbf{Q}_L$ ,  $t = 26$  (forced oscillations mode) and  $t = 55$  (free oscillations mode).

$U_0^i(g,t)$  and  $U_0(g,t)$  waves. The spatial distribution of values  $E_x(g,t)$ ,  $g \in \mathbf{Q}_L$  corresponding to the field  $U(g,t)$  is governed equally by all these waves. At some points in time there is practically no difference in the distribution (at  $k = k_{\pm 1}^+$ ) due to the interference of sinusoidal waves  $\tilde{U}_0^i(g,k)$  and  $\tilde{U}_n(g,k)$ ,  $n = 0, \pm 1$ . The distinctions decrease monotonically with time  $t$ , provided that the central frequency  $\bar{k}$  of quasi-monochromatic wave  $U_0^i(g,t)$  (with a sufficiently large spatial duration  $\bar{T}$ ) coincides exactly with  $k_{\pm 1}^+$ . Thus in this situation, the principle of limiting amplitude [3] is realized, and the transient gradually takes on properties of the established process.

Now let us excite a symmetrical echelette grating with an  $E$ -polarized wideband signal  $U_0^i(g,t)$  [see Fig. 9(a): the bandwidth is given by  $0.4 < k < 2.8$ , where normalized spectral amplitudes of the function  $v_0(L_1,t)$  are no less than 0.1]. The spectral amplitudes of the pulses  $u_0(L_1,t)$  and  $v_0(L_1,t)$  differ little from each other everywhere except in the frequency interval beyond the threshold point  $k_{\pm 1}^+$ . Amplitudes of pulses  $u_{\pm 1}(L_1,t)$  are at their maxima on this frequency interval. As in the case of a grating excitation by a monochromatic signal  $U_0^i(g,t)$  all features of the functions  $u_n(L_1,t)$  and  $|\tilde{u}_n(L_1,k)|$  originate from the threshold effect in the frequency domain and the redistribution of the input energy among the spatial harmonics of the field  $\tilde{U}^s(g,k)$ .

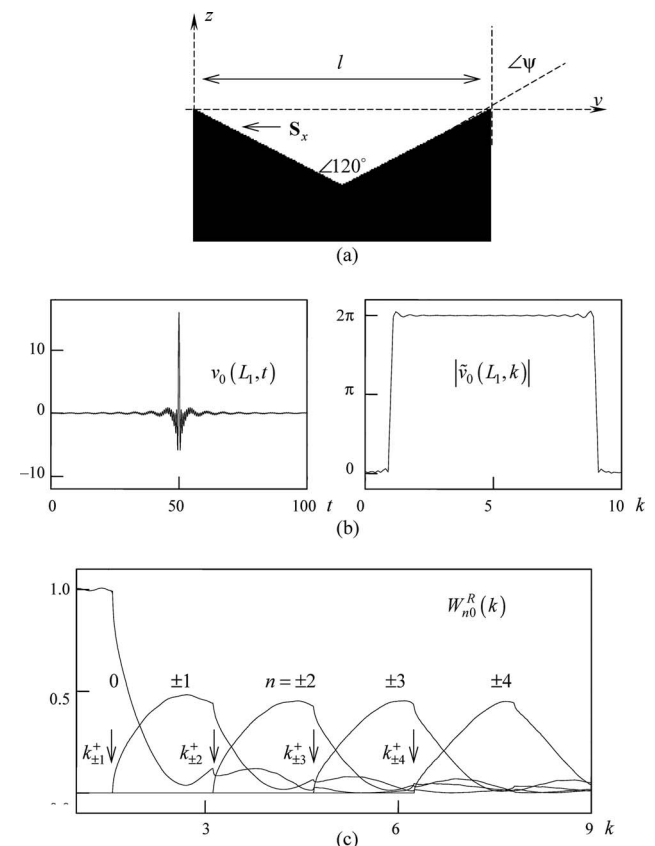


Fig. 10. Mode-frequency exfoliation of a superbroadband pulse: (a) Grating geometry ( $\psi = 60^\circ$ ,  $l = 4.02$ ,  $L_1 = 8.0$ ); (b) amplitudes of the incident  $E$ -polarized pulsed wave  $U_0^i(g,t)$  ( $\Phi = 0$ ); (c) energy distribution among spatial harmonics of the field  $\tilde{U}^s(g,k)$  in the structure's reflection zone.

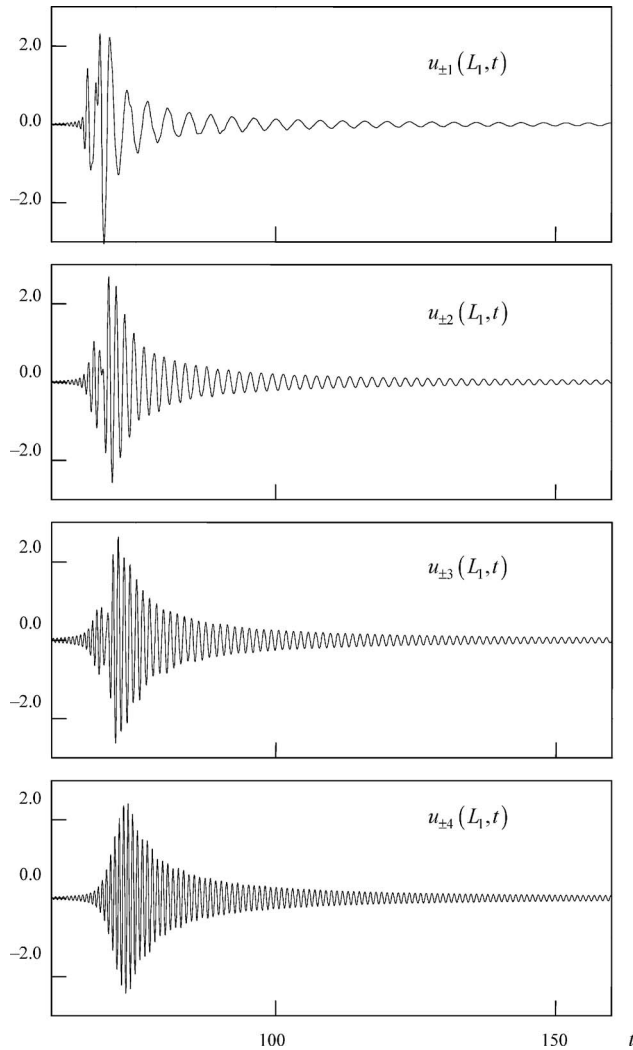


Fig. 11. (Complement to Fig. 10). Amplitudes of high-order spatial harmonics of the field  $U^s(g, t)$  on the virtual boundary  $L_1$ .

Now consider the *phenomenon of the strong conversion of the sinusoidal  $H_{01}$ -waves into the  $H_{0m}$ -waves*,  $m > 1$  that takes place on inclined  $H$ -plane plugs in rectangular waveguides (see Fig. 12 in [15]). This can be interpreted in superwideband signal terms in the following manner. The pulsed  $H_{01}$ -wave with spectral amplitudes evenly distributed across the range  $k_2 < k < k_M$  ( $k_m$  is the  $H_{0m}$ -wave cutoff) is reflected from the plug to produce a series of pulsed  $H_{0m}$ -waves,  $m = 2, \dots, M-2$ , each occupying its own band  $k_m < k < k_{m+2}$  in the range. In this band, function  $W_{m1}(k)$  describing the input energy portion transferred to the reflected  $H_{0m}$ -wave at first monotonically increases from zero up to  $\max_k W_{m1}(k) = W_{m1}(k_{m+1}) \approx 1$ , then monotonically decreases to  $W_{m1}(k_{m+2}) \ll 1$ .

Phenomena of this kind appear during scattering of superwideband  $TE_{01}$ -pulses on cone-shaped plugs in circular and coaxial waveguides [16] and also during scattering of  $E$ -polarized pulsed waves of normal incidence on a symmetric metal echelette grating with obtuse teeth (see Figs. 10 and 11). The result is that a superwideband pulse of one type [for echelette gratings, it is the pulsed wave  $U_0^i(g, t)$ ] changes into an ordered sequence of narrowband pulses of other types [pulsed spatial harmonics  $U_n(g, t)$ ;

$|n| \geq 1$ ]. This effect is called *modal frequency exfoliation of a superwideband signal*. Particular bands occupied by each pair  $U_{\pm n}(g, t)$  of pulsed waves and the  $W_{n0}(k) = W_{-n0}^R(k) + W_{n0}^R(k)$  distributions across these bands remain basically the same as in the case of  $H_{0n}$ -waves of a rectangular waveguide. The reflected pulses  $U_{\pm n}(g, t)$  with a higher  $|n|$  have a higher central frequency  $\tilde{k}_n \approx k_{\pm(n+1)}^+$ . This can be seen clearly in the character of the oscillations of the spatial-temporal amplitudes  $u_{\pm n}(z, t)$  as a function of  $t$  (see Fig. 11).

In the case of  $H$ -polarization the effect is not so obvious. Formation of pairs  $U_{\pm n}(g, t)$  of the reflected pulses fitting the above-given notion of modal frequency exfoliation starts only beyond the point  $k = k_{\pm 3}^+$ —the grazing point for the plus and minus third spatial harmonics of the field  $\tilde{U}^s(g, k)$ . But now the top value of the energy characteristic  $W_{n0}(k)$  cannot reach over a 0.85 level for any of the pairs. Distinctions from the  $E$ -case are mainly due to different intensities of the threshold phenomenon (Wood's anomalies) in the vicinities of the first three branch points  $k = k_{\pm n}^+$ .

## 5. CONCLUSION

Some physical results obtained by the method described in [1] are briefly depicted in this paper. These results concern spatial-temporal and spatial-frequency field transformations in the case of resonant wave scattering. They underscore the potentialities of this method and its prospects as a research tool for fundamental and application-oriented problems of physics and optics.

## REFERENCES

1. K. Y. Sirenko, Y. K. Sirenko, and N. P. Yashina, "Modeling and analysis of transients in periodic gratings. I. Fully absorbing boundaries for 2-D open problems," *J. Opt. Soc. Am. A* **27**, 532–543 (2010).
2. A. Taflov and S. C. Hagness, *Computational Electrodynamics: the Finite-Difference Time-Domain Method* (Artech House, 2000).
3. Y. K. Sirenko, S. Strom, and N. P. Yashina, *Modeling and Analysis of Transient Processes in Open Resonant Structures. New Methods and Techniques* (Springer, 2007).
4. O. A. Ladyzhenskaya, *The Boundary Value Problems of Mathematical Physics* (Springer-Verlag, 1985).
5. B. Engquist and A. Majda, "Absorbing boundary conditions for the numerical simulation of waves," *Math. Comput.* **31**, 629–651 (1977).
6. G. Mur, "Absorbing boundary conditions for the finite difference approximation of the time-domain electromagnetic-field equations," *Int. J. Remote Sens.* **23**, 377–382 (1981).
7. Y. K. Sirenko and N. P. Yashina, "Nonstationary model problems for waveguide open resonator theory," *Electromagnetics* **19**, 419–442 (1999).
8. Y. K. Sirenko and N. P. Yashina, "Time domain theory of open waveguide resonators: canonical problems and a generalized matrix technique," *Radio Sci.* **38**, VIC 26-1–VIC 26-12 (2003).

9. V. P. Shestopalov, L. N. Litvinenko, S. A. Masalov, and V. G. Sologub, *Wave Diffraction by Gratings* (Kharkov State Univ. Press, 1973) (in Russian).
10. R. Petit, ed., *Electromagnetic Theory of Gratings* (Springer-Verlag, 1980).
11. V. P. Shestopalov, A. A. Kirilenko, S. A. Masalov, and Y. K. Sirenko, "Diffraction gratings," in *Resonance Wave Scattering*, Vol. 1 (Naukova Dumka, 1986) (in Russian).
12. V. P. Shestopalov and Y. K. Sirenko, *Dynamic Theory of Gratings* (Naukova Dumka, 1989) (in Russian).
13. L. G. Velychko, Y. K. Sirenko, and O. S. Shafalyuk, "Time-domain analysis of open resonators. Analytical grounds," *PIER* **61**, 1–26 (2006).
14. A. O. Perov, Y. K. Sirenko, and N. P. Yashina, "Periodic open resonators: peculiarities of pulse scattering and spectral features," *PIER* **46**, 33–75 (2004).
15. V. P. Shestopalov, A. A. Kirilenko, and L. A. Rud', "Waveguide discontinuities," in *Resonance Wave Scattering*, Vol. 2 (Naukova Dumka, 1986) (in Russian).
16. K. Y. Sirenko, "Splitting of super-broadband pulses by simple inhomogeneities of circular and coaxial waveguide," *Telecommun. Radio Eng.* **67**, 1415–1428 (2008).